Optogeometric Study of Multimode TiO2 Waveguide Thin Films Elaborated by Reactive Magnetron Sputtering

Article *in* SSRN Electronic Journal · January 2022

DOI: 10.2139/ssrn.4022367

CITATIONS
0

READS
81

10 authors, including:

Abdelouadoud Mammeri
University of Constantine 1
8 PUBLICATIONS **2** CITATIONS
SEE PROFILE

Serrar Hacene
Research Center In Industrial Technologies
20 PUBLICATIONS **50** CITATIONS
SEE PROFILE

Boulkra Mohamed
Badji Mokhtar - Annaba University
6 PUBLICATIONS **11** CITATIONS
SEE PROFILE

Nezzari Hassene
Research Center In Industrial Technologies
12 PUBLICATIONS **33** CITATIONS
SEE PROFILE

Optogeometric study of multimode TiO_2 waveguide thin films elaborated by reactive magnetron sputtering

Abdelouadoud Mammeri [*1], Yassine Bouachiba[2], Aabderrahmane Bouabellou[1], Hacene Serrar[3], Khaled Laggoune[3], Ilyes Sekhri[4], Adel Taabouche[1], Badis Rahal[5], Mohamed Boulkra[3], and Hassene Nezzari[6]

[1]Laboratoire Couches Minces et Interfaces, Université de Fréres Mentouri Constantine 1, Constantine, Algérie.

[2]Laboratoire Technologie des Matériaux Avancés, Ecole Nationale Polytechnique de Constantine Malek BENNABI,BP 75A RP, Ali Mendjeli, Constantine, Algérie.

[3]Research Center in Industrial Technologies (CRTI), BP 64 Cheraga, Alger, Algeria.

[4]Laboratoire Dosage, Analyse et Caractérisation en Haute Résolution, Université Ferhat Abbas, Sétif, Algérie.

[5]Nuclear Techniques Division, Nuclear Research Center of Algiers, 2 Bd, Frantz Fanon, BP 399, 16000, Algiers, Algeria.

[6]Département de Génie Electrique, Faculté des Sciences et la Technologie, Université Larbi Tebessi, Tebessa.

February 21, 2022

[*]corresponding author: abdelouadoud.mammeri@gmail.com

Abstract

TiO_2 thin films were deposited by reactive magnetron sputtering with increasing thickness T_1, T_2 , T_3 and T_4. The μ-Raman spectra showed the presence of anatase TiO_2 in all films. The phonon confinement model revealed the crystallite size ranging between 5.9 and 6.1 nm. The gap energy was found to decrease from 3.45 eV to 3.37 eV. SEM and EDX analysis showed that the crystallinity and stoichiometry of T_4 were enhanced in comparison to T_1. The m-lines spectroscopy confirmed the normal behavior of the films as multimode waveguide by the increase of the number of propagation modes with films' thickness for each Transverse Electric and Transverse Magnetic polarization. Both ordinary and extraordinary refractive indices decreased over films' thickness, the birefringence however had an opposite behavior. The cut-off thickness experienced an increment as a function of thickness. In comparison, m-lines and Swanepoel's method were relatively compatible.

Keywords: Multimode waveguide, TiO_2, refractive index, birefringence, cut-off thickness, prism coupler.

1 Introduction

Titanium dioxide (TiO_2) is a dielectric with three allotropes: anatase (tetragonal), rutile (tetragonal) and brookite (orthorhombic). In addition to its low coast, it has very intriguing optical and chemical properties including high refraction index and dielectric constant, low extinction coefficient in the infrared and the visible region, high resistance to photocorrosion, non-toxicity and bio-compatibility [1–4], large optical nonlinearity and negative thermo-optic coefficient [5]. Consequently, TiO_2 found use as low lost optical waveguide [6], integrated optical amplifier [7], optical communication device, sensor [8] and antireflection coating [9] as well as an industrial pigment [10]. Many preparation procedures for TiO_2 thin films were reported including reactive magnetron sputtering [7]. Reactive magnetron sputtering is an effective deposition technique for uniform large scale coating with high quality film and strong substrate adhesion [11].

Thin films optical waveguides continue to thrive as it bears strong potential for application in bio and chemical sensing [12–14]. These sensors differ in their operating principle and we mention: Surface Plasmon Resonance (SPR), resonators, and interferometers. The latter received much attention and development as a multimode interferometer sensor [15]. The thickness of the waveguide is intimately related to numerous number of its properties and functionalities including sensitivity, porosity and dielectric behavior [16–19] . Waveguides with a thickness larger than the wavelength of

the coupled light (several microns) permit the possibility of multimodes propagation. The material used to fabricate them are typically glass, polymer or silica which renders them relatively inexpensive and simple to manufacture [14]. Using high refractive index material such as TiO_2 allows for thinner waveguides with the same propagation modes in addition to the privileges offered by the material properties mentioned above.

In order to design such a waveguide, the variation of its optical properties, for instance, the refractive index, birefringence, cut-off thickness, effective index and the modes of propagation as a function of thickness must be understood and considered.

In this work, we concerned ourselves with the study of the effect of thickness on the structural, morphological and optical properties with an emphasis on the waveguide properties of TiO_2 thin films on the basis of prism coupler measurements with comparison to Swanepoel's method.

2 Experimental

2.1 Deposition conditions and characterization techniques

Reactive magnetron sputtering deposition was used to deposit titanium dioxide (TiO_2) onto ordinary glass microscope slides. The target was titanium metal disc of 99.99% purity and the reactive gas was therefore oxygen. The pressure of the chamber was kept very close to $10^{-6}\ torr$ with 20:8 argon to oxygen ratio. The power used in this setup was $250\ W$ and the glass substrates were heated to 350 °C. During the deposition process, the substrate was under constant $3\ rpm$ rotation, at $5\ cm$ distance from the target and a deposition rate of $2\ nm/s$.

To proceed with this work, the elaborated films were investigated using several techniques. For the structural properties μ-Raman spectra were recorded at room temperature by inVia Confocal Raman Microspectrometer at an excitation wavelength of 632.8 nm. For the optical and waveguide properties of the films, Metricon 2010/M-lines based Prism Coupler (rutile TiO_2: n_e=2.8639, n_o=2.5822 and an apical angle of 44.60°) was employed to couple 632.8 nm HeNe laser light into air/TiO_2/glass in addition to Shimadzu UV-3101PC Spectrophotometer for transmittance evaluation. Finally scanning electron microscope and energy dispersive X-ray spectroscopy (JEOL JSM-7001F) for surface morphology and stoichiometry respectively. The thickness of the films was measured using m-lines and abbreviated in the next table:

Table 1: Thin film name abbreviation with respect to thickness (TE).

Sample	Thickness (nm)
T_1	137
T_2	284
T_3	441
T_4	661

2.2 Phonon confinement model

For a better understanding of the structural properties of TiO_2. The phonon confinement model was adopted [20, 21]. In an ideal crystal, the scattering of a phonon is due to the Raman active optical phonons close to the Brillouin zone center Γ. In a nanocrystal of a diameter less than 10 nm, the phonon will be localized within the dimensions of the crystallites [22]. A confined phonon in a supposedly spherical nanocrystal of a diameter L is described by its wave function $\psi(\vec{q_0}, \vec{r})$ as follows:

$$\psi(\vec{q_0}, \vec{r}) = W(\vec{r}, L)u(\vec{q_0}, \vec{r})e^{-\vec{q_0}\cdot\vec{r}} \tag{1}$$

where $W(\vec{r}, L)$ is the confinement function and $u(\vec{q_0}, \vec{r})$ contains the periodicity of the lattice. The Raman intensity as a function of wave number can be calculated over a spherical Brillouin Zone (BZ) of TiO_2 ($a = 0.3768$ nm) using the following equation:

$$I(\omega) \propto \int_{BZ} \frac{\|c(\vec{q_0}, \vec{q})\|^2}{(\omega - \omega(\vec{q}))^2 + (\frac{\Gamma_0}{2})^2} d^3\vec{q} \tag{2}$$

where Γ_0 is the full width at half maximum of the Raman peak of anatase particles at room temperature with the value of 7 cm^{-1}, $\omega(\vec{q})$ is the phonon dispersion curve of the intense E_g mode and $\|c(\vec{q_0}, \vec{q})\|^2$ is the Fourier coefficients of the expansion of $\psi(\vec{q_0}, \vec{r})$ around the BZ center [23]. The dispersion curve was taken to be parabolic $\omega(\vec{q}) = \omega_0 + b\vec{q}^{\,2}$, where $\omega_0 = 142.9$ cm^{-1} and $b = 2.23$ [20, 21, 23].

The Fourier coefficients are commonly expressed as Gaussian peak function $\|c(0, \vec{q})\|^2 = e^{(\frac{-\vec{q}^{\,2}L^2}{48\pi^2})}$ ($\vec{q_0} = 0$ at the center of BZ), however, it was not a good fit for our data instead, an analogy to the ground state of an electron in hard sphere confinement function was adopted [24, 25]

$$\|c(0, \vec{q})\|^2 = \frac{\sin^2(\frac{qL}{2})}{(4\pi^2 - q^2L^2)^2} \tag{3}$$

2.3 M-lines: theoretical considerations

Prism coupler or so-called m-lines is a technique that uses a prism of high refractive index to couple light into at least tree layered system, in our case air/TiO_2/glass (n_{TiO_2}>n_{glass}>n_{air}). This coupling is possible via an evanescent tail of a monochromatic light reflected by the prism's base. When the layer (air) between the waveguide (TiO_2) and the prism's base is about a quarter of the wavelength of the measurement light and the tangential propagation constants of the light in the prism and the mode in the waveguide are equal. The light will be coupled in the waveguide and a drop in the intensity of the reflected light is observed. In the frame of geometrical optics and using Snell–Descartes law, the effective index (n_{eff}) of the mode m is expressed in terms of the prism's index of refraction n_p, the positive angle of incidence (θ) with respect to the normal of the prism's face and the prism's base angle (θ_p) as [26–29]:

$$n_{eff} = n_p \sin\left(\arcsin\left(\frac{n_a \sin(\theta)}{n_p}\right) + \theta_p\right) \tag{4}$$

therefore by varying the angle θ one can excite multiple propagation modes. The dispersion curves of the TiO_2 waveguide films for each Transverse Electric (TE, equation 5) and Transverse Magnetic (TM, equation 6) polarization are the equations connecting the films' thickness and the effective index. These equations stem from Maxwell equations applied to the boundary conditions for an isotropic slob waveguide and gives out the following equations [26–28]:

$$k_0 d\sqrt{n^2 - n_{eff}^2} = \arctan\left(\sqrt{\frac{n_{eff}^2 - n_a^2}{n^2 - n_{eff}^2}}\right) + \arctan\left(\sqrt{\frac{n_{eff}^2 - n_s^2}{n^2 - n_{eff}^2}}\right) + m\pi \tag{5}$$

$$k_0 d\sqrt{n^2 - n_{eff}^2} = \arctan\left(\frac{n^2}{n_a^2}\sqrt{\frac{n_{eff}^2 - n_a^2}{n^2 - n_{eff}^2}}\right) + \arctan\left(\frac{n^2}{n_s^2}\sqrt{\frac{n_{eff}^2 - n_s^2}{n^2 - n_{eff}^2}}\right) + m\pi \tag{6}$$

where $k_0 = \frac{2\pi}{\lambda}$, λ is the wavelength of the radiation source ($632.8\ nm$), d is the film thickness, n is the refractive index of the film, m is the mode number, n_a and n_s are the refractive indices of the superstrate and the substrate respectively. In our case the superstrate was air and the substrate was ordinary glass.

2.4 Swanepoel's Method

The method was established by Swanepoel [30] and it is based on the use of transmittance spectrum to calculate the complex refractive index of a transparent thin film. The transmitted beam through the film and the substrate is assumed to be normal to the surface of incidence. The interference caused by the multiple refraction at the two interfaces namely film/substrate and air/film can be seen as a fringes pattern in the transmittance spectra. The thickness of the substrate must be several orders of

magnitude than that of the film. For a thin film of a very small extinction coefficient the transmittance can be written as:

$$T(\lambda) = \frac{A\beta}{B - C\beta\cos\theta + D\beta^2} \tag{7}$$

where
$A = 16n^2 n_s$, $B = (n+1)^3(n+n_s^2)$, $C = 2(n^2-1)(n^2-n_s^2)$, $D = (n-1)^3(n-n_s^2)$, $\theta = \frac{4\pi nd}{\lambda}$ and $\beta = \exp(-\alpha d)$. n is the refractive index of the film, n_s is the refractive index of the substrate, d is the thickness of the film, θ is the phase difference between the direct beam ($\vec{b}_d$) and the multiple reflected beam ($\vec{b}_r$) and α is the absorption coefficient. The path difference between $\vec{b}_d$ and $\vec{b}_r$ is of the following:

$$2nd = m\lambda \tag{8}$$

the constructive and destructive interference will occur for m being a full integer and half an integer respectively. In the light of the work of Manifacier et al. [31] we can use continuous functions of λ as envelopes of the maxima T_M and the minima T_m of the transmission spectrum:

$$T_M = \frac{A\beta}{B - C\beta + D\beta^2} \tag{9}$$

$$T_m = \frac{A\beta}{B + C\beta + D\beta^2} \tag{10}$$

combining the reciprocal of equations 9 and 10 yields:

$$\frac{1}{T_m} - \frac{1}{T_M} = \frac{2C}{A} \tag{11}$$

by direct substitution of A and C we can calculate the refractive index such that:

$$n = \sqrt{N + \sqrt{N^2 - n_s^2}} \tag{12}$$

depending on the absorption coefficient, equation 12 will change. For the transparent region N will be:

$$N = \frac{2n_s}{T_m} + \frac{n_s^2 + 1}{2} \tag{13}$$

and for the weak and medium absorbing region:

$$N = 2n_s\frac{T_M - T_m}{T_m \cdot T_M} + \frac{n_s^2 + 1}{2} \tag{14}$$

the equation for the refractive index of the substrate n_s can be calculated using the following equation:

$$n_s = \frac{1}{T_s} + \sqrt{\frac{1}{T_s} - 1} \tag{15}$$

The refractive index is now a function of T_M and T_m. Equation 8 for two successive maxima or minima, refractive indices n_1 and n_2 and wavelengths of λ_1 and λ_2 ($\lambda_1 > \lambda_2$) can be written as:

$$\begin{aligned} 2dn_1 &= m\lambda_1 \\ 2dn_2 &= (m+1)\lambda_2 \end{aligned} \tag{16}$$

so we can solve for the thickness d

$$d = \frac{\lambda_1\lambda_2}{2(\lambda_1 n_2 - \lambda_2 n_1)} \tag{17}$$

The envelop functions were calculated using OriginPro 2016 (Origin- Lab Corp.). In summary the method will proceed as follows: Computing the envelope function T_M and T_m starting from the transmittance data. For a particular wavelength (λ) there exists a maxima on the transmittance spectrum (or equivalently T_M) and a corresponding minima on the envelope T_m and vice versa. These points will be used in equation 12 to calculate the refractive index (n) and hence the thickness (d) [32, 33].

3 Results and discussion

3.1 Raman spectroscopy

In order to identify the crystal structure of the TiO_2 thin film, the μ-Raman spectroscopy was used and the spectra were displayed in figure 1. The intensity in the interval 190-800 cm^{-1} of T_2, T_3 and T_4 thin films was rescaled with respect to the intensity of E_g peak for more visibility of the peaks present in the same interval. Anatase TiO_2 has six atoms per unit cell so there are fifteen optical vibrational modes: $1A_{1g} + 1A_{2u} + 2B_{1g} + 1B_{2u} + 3E_g + 2E_u$ [34, 35], six of which are Raman active [36] namely 144 (E_g) , 197 (E_g), 399 (B_{1g}), 513 (A_{1g}), 519 (B_{1g}) and 639 cm^{-1} (E_g). In the case of TiO_2 rutile structure the fundamental modes are 143 (B_{1g}), 447 (E_g), 612 (A_{1g}), and 826 cm^{-1} (B_{1g}) [37]. It is obvious from figure 1 that the T_1 thin film had poor anatase crystallinity. The anatase structure was also present in the thicker films (T_2, T_3 and T_4), however, the T_3 film exhibited small traces of the rutile phase. The vibration modes positions in addition to the crystallite sizes deduced from the phonon confinement model were depicted in table 2. The blue shift and broadening of the peaks were therefore attributed to phonon confinement as the main cause [38] in addition to non-stoichiometry defects [39, 40].

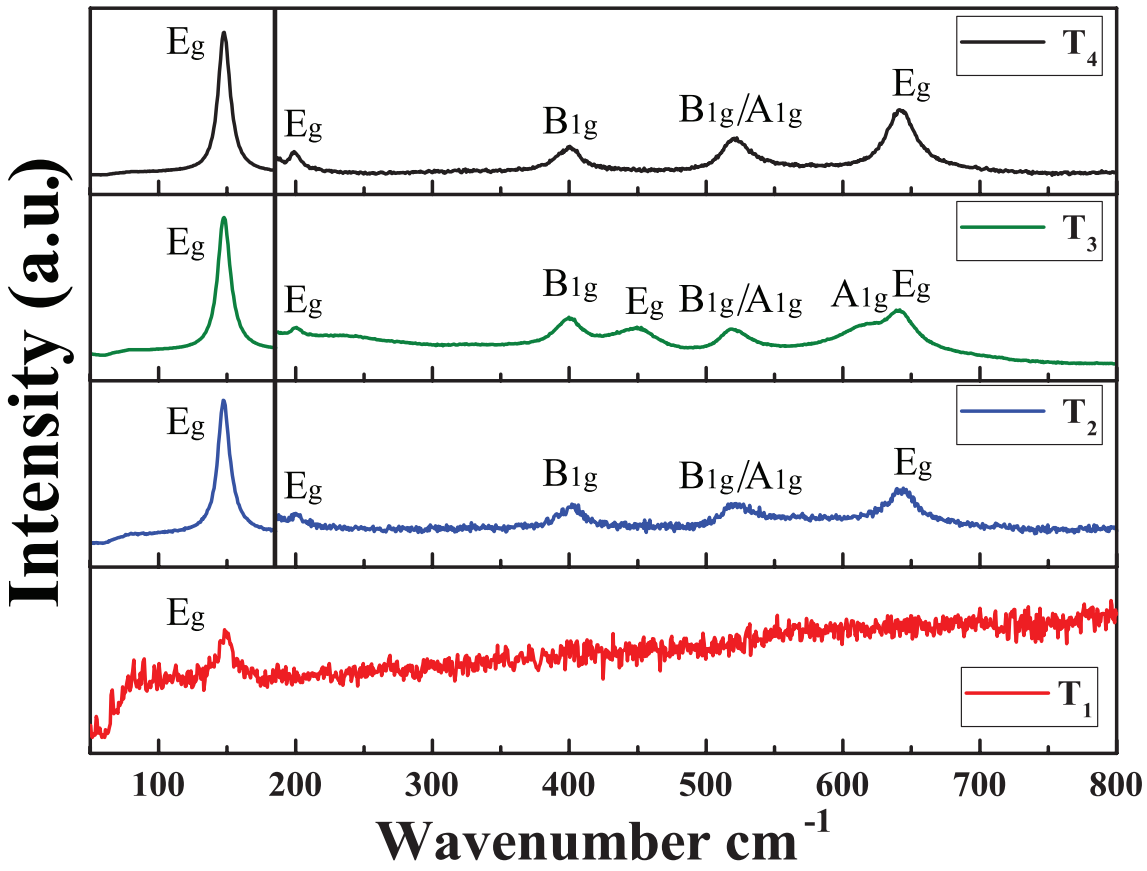

Figure 1: The Raman spectra of the as-deposited thin films.

Table 2: Obtained and calculated information from the μ-Raman spectra.

Peak		T_1 Peak position (cm^{-1})	T_2 Peak positions (cm^{-1})	T_3 Peak positions (cm^{-1})	T_4 Peak positions (cm^{-1})
Anatase	E_g	149	149	149	149
Anatase	E_g	/	201	202	201
Anatase	B_{1g}	/	403	402	402
Rutile	E_g	/	/	447	/
Anatase	A_{1g}/B_{1g}	/	525	523	524
Rutile	A_{1g}	/	/	617	/
Anatase	E_g	/	643	643	643
Crystallite size (nm)		5.1	5.9	5.9	6.1

3.2 UV-Vis

The transmittance spectra of the TiO_2 thin films were depicted in figure 2. There was no significant change in the average transmittance of the thin films over the visible region (400-800 nm). The results calculated by Swanepoel's method were listed in table 3. A red shift was present in the absorption

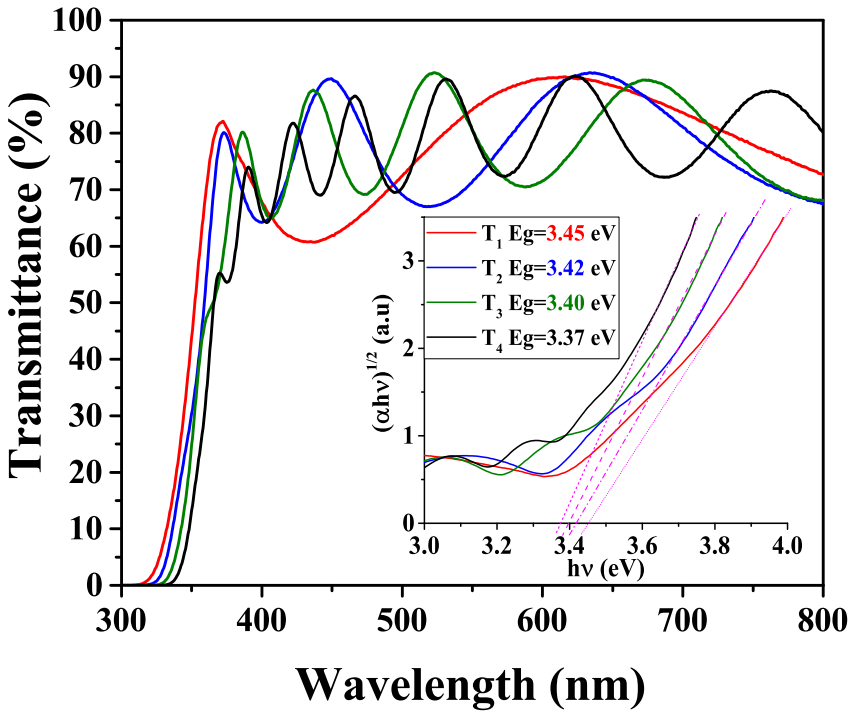

Figure 2: Transmittance spectra and tauc's plots for the various deposited thin films.

edge as the thickness increased. This shift was obvious in the optical gap energy which was calculated by linear extrapolation of the plot $(\alpha h\nu)^{\frac{1}{2}}$ vs. photon energy $(h\nu)$ using Tauc's equation [41]:

$$\alpha h\nu \propto (h\nu - E_g)^n \tag{18}$$

where h is the plank's constant, ν is the frequency of the photon, E_g is the optical gap energy, α is the absorption coefficient and n equals 2 for indirect allowed transition in the case of anatase TiO_2. From previous studies, the anatase TiO_2 thin films optical gap energy takes values of 3.15 to 3.4 eV [42]. The optical gap energies of our obtained thin films were close to the above mentioned range. However, these values were still higher than that of the single crystal bulk (3.18 eV [43]) which was attributed to quantum size effects [44, 45]. The increase in the films' thickness slightly reduced the quantum size effects and therefore lowered the optical gap energy. Furthermore, the widening in the optical band gap could be attributed to the non-stoichiometry of the films since stoichiometry has a direct effect on the electronic structure of compounds [46, 47] and the lack of Ti atoms will mainly result in a decrease in the isolated Ti $3d_{xy}$ electronic state which is the minimum of the conduction band [48, 49]. This effect will be justified in the next section via EDX analysis.

3.3 Surface morphology and composition

Scanning Electron Microscope imaging (SEM figure 3) in addition to Energy Dispersive X-ray spectroscopy (EDX figure 4) were performed on the T_1 and the T_4 thin films. The T_1 film had small dispersed grains (less than 40 nm on average) of poorly crystallized anatase structure [50] in accordance with EDX analysis which indicated $\frac{80}{19}$ oxygen to titanium atomic ratio. The T_4 thin film had relatively homogeneous spherical grains which meant that the film exhibited a better crystallinity with an average grain size of 100 nm [51]. This latter had $\frac{62}{37}$ oxygen to titanium atomic ratio which was close to the perfect stoichiometry of TiO_2. These observations seem to be in good agreement with μ-Raman and UV-Vis results [39, 40].

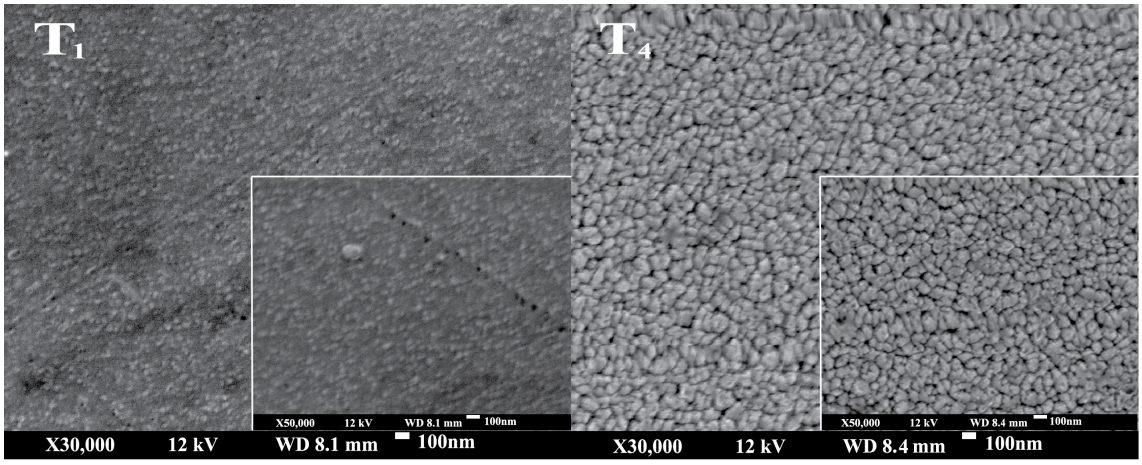

Figure 3: Scanning electron microscope images of the T_1 (left) and T_4 (right) thin films.

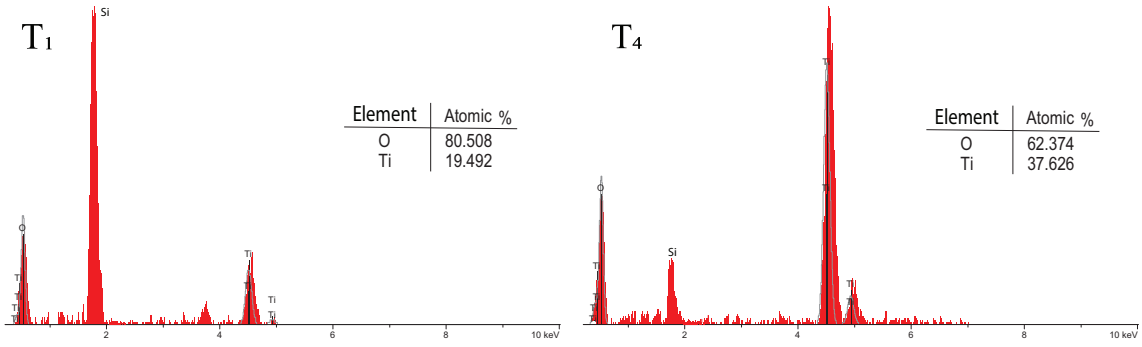

Figure 4: Energy dispersive X-ray spectroscopy peaks in addition to the stoichiometry of T_1 (left) and T_4 (right) thin films.

3.4 M-lines measurements

The waveguiding curves were presented in figure 5. It was notable that the optical guided modes number increased with thickness. The ordinary refractive index (n_o) and the thickness (d) of the film

were calculated simultaneously by solving equation 5 for at least two modes and in the same manner, the extraordinary refractive index (n_e) and the thickness were obtained from equation 6 [52]. Both ordinary and extraordinary refractive indices as well as the beirefringence were depicted in figure 6.

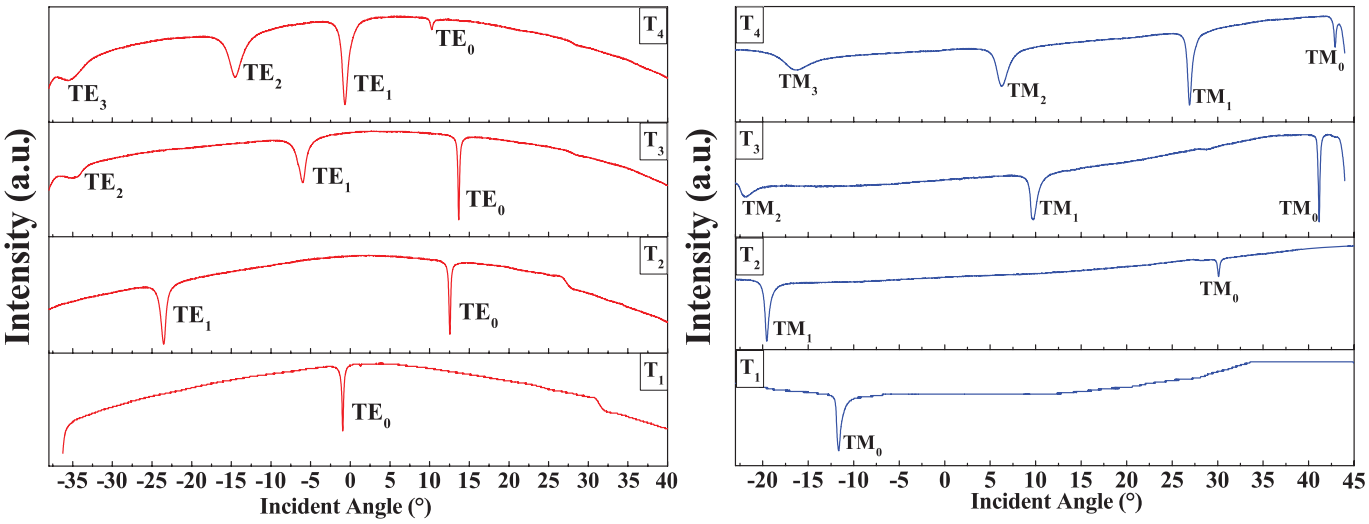

Figure 5: The reflected intensity from the base of the prism as a function of the angle of incidence, TE polarization (left) and TM polarization (right).

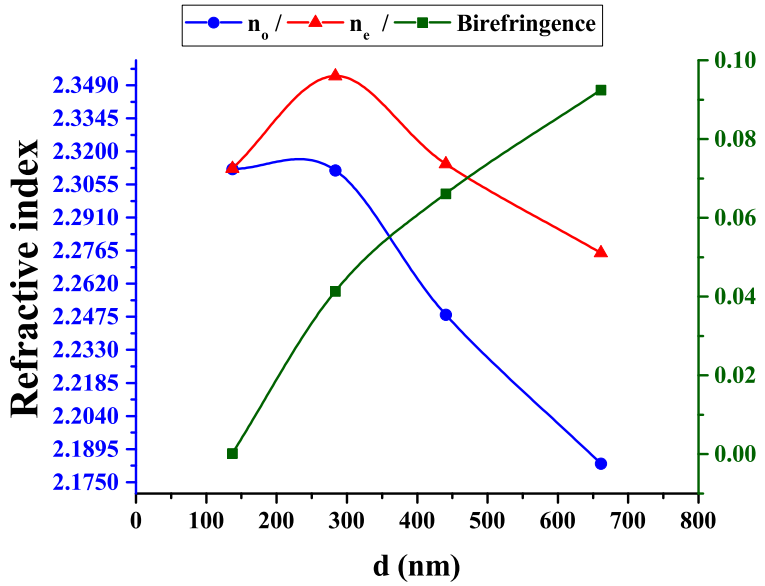

Figure 6: The variation of the ordinary (n_o), extraordinary (n_e) refractive indices and birefringence as a function of films' thickness.

To explain the relation between the refractive index and the density of crystals a modified expressions of Gladstone–Dale relation were proposed [53, 54]. On that account, we can state clearly that

the diminishing in the density of the thin films leads to a diminishing in the refractive index. This was put to use to explain the slight decrease of the refractive indices as a function of thickness (figure 6) and it is in perfect agreement with the work of Rocquefelte et al. [55] on the major effect of density of different TiO_2 crystal structures on their refractive index. The main reason for the decrease in density as the thickness increased and therefore the refractive index was the deposition method namely reactive magnetron sputtering as the density of the sputtered films is proportional to the inverse of the thickness as investigated by Swann [56].

The birefringence ($\Delta n = n_e - n_o$) of the T_1 thin film was almost zero which was due to the fact that the film had a poor anatase crystallinity so the anisotropy was lost (figure 6). The rest of the thin films experienced an increase in the birefringence as they approached more and more the bulk state [57]. The difference in birefringence between the films and that of the bulk (0.073) was an indication of change in the Ti-O bond polarizability in the two main directions of the anatase structure [58–60].

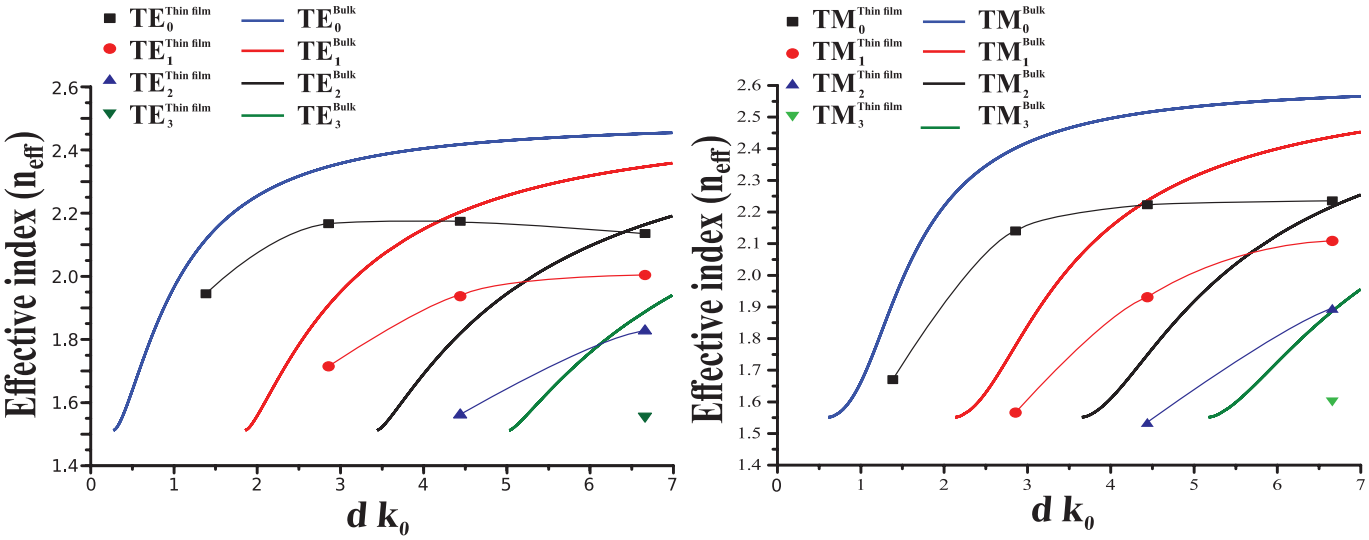

Figure 7: The dispersion curves: the solid lines represent the bulk index of refraction, the connected dots represents the obtained thin films' refractive indices.

Equations 5 and 6 were plotted with respect to the optical anisotropic nature of anatase TiO_2 in figure 7, which depicted the evolution of effective indices vs. thickness for n being that of the bulk and our thin films. The ordinary refractive index of bulk anatase TiO_2, and the extraordinary one were taken to be $n_o = 2.488$ and $n_e = 2.561$ respectively [61]. The effective index as a function of thickness in both TE and TM polarization was in qualitative accordance with dispersion curves of bulk anatase TiO_2 indicating the normal behavior of the films as a slob waveguide, nonetheless, there were not a very high quantitative agreement. This was explained provoking the relation between the density

and thickness as discussed above i.e, the effective indices of the obtained thin films were smaller in value than that of the bulk. As had been previously mentioned, the T_4 thin film exhibited eight modes, four in each TE and TM polarization. The number of modes decreased with the decrease in the films' thickness (figure 5). This is expressed in the cut-off condition which indicates the minimum thickness (d_{min}) needed to support a mode m in a thin film [26]:

$$d_{min}(TE) = \frac{\arctan\left(\sqrt{\frac{n_s^2-n_a^2}{n^2-n_a^2}}\right) + m\pi}{k_0\sqrt{n^2-n_a^2}} \tag{19}$$

$$d_{min}(TM) = \frac{\arctan\left(\frac{n^2}{n_a^2}\sqrt{\frac{n_s^2-n_a^2}{n^2-n_a^2}}\right) + m\pi}{k_0\sqrt{n^2-n_a^2}} \tag{20}$$

the minimum thickness d_{min} is supposed to be only a function of the mode number m, despite that the refractive index n in equations 19 and 20 was it self a function of thickness, therefore the minimum thickness for each propagating mode will get affected by the film thickness. Figure 8 illustrates d_{min} as a function of mode number m for the bulk refractive index in addition to the refractive indices obtained for our thin films. It was seen clearly that the increase in thickness of the films decreased the refractive index which in its turn increased the cut-off thickness. This is very important to consider when designing thin films for waveguiding.

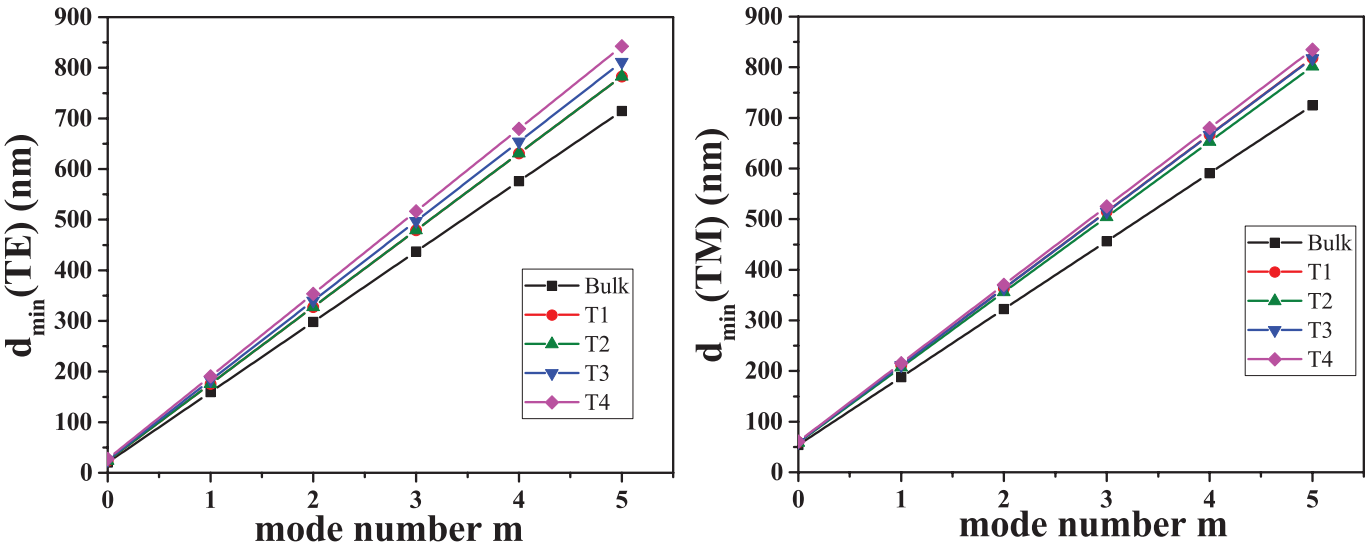

Figure 8: The cut-off condition as a function of the mode number m and the refractive indices n.

The calculated refractive index obtained by Swanepoel's method in the weak absorption region was fitted using the full Cauchy's equation [62] or just taking the two first terms to obtain table 3, accordingly the refractive index was determined from the fitted plot at $\lambda = 632.8\ nm$. The thickness

of the films calculated by the same method were slightly different in comparison with those measured by m-lines measurements. The fitted results of the refractive index based on Swanepoel's data were found generally to decrease with the increase in thickness which was in alignment with previous explanations. We justified the difference between the two methods by mentioning the fact that Swanepoel's method relay on the transmittance measurement which was performed using unpolarized light, consequently the detector of the UV-Vis instrument will detect the average interaction of the incident light with the thin film. Contrary to m-lines which is founded on the selective excitation through an evanescent field of guided modes of a film by varying the angle of incident as previously mentioned. This permits more accurate evaluation of propagation constant in the film and hence the refractive index.

Table 3: The information obtained and calculated from Swanepoel's method and m-lines.

Sample	Prism coupler measurements			Swanepoel's method calculations	
	n_o	n_e	Thickness (nm)	refractive index	Thickness (nm)
T_1	2.3123	2.3125	137	2.168	163
T_2	2.3117	2.3530	284	2.263	377
T_3	2.2484	2.3145	441	2.150	420
T_4	2.1831	2.2755	661	2.105	754

4 Conclusion

In this work, we had investigated the effect of thickness on the various properties of $\mathrm{TiO_2}$ thin films prepared by magnetron reactive sputtering. The μ-Raman spectra showed that all films exhibited anatase structure. The optical gap energy was found to decrease over the increase in thickness.
The optical properties were determined by m-lines spectroscopy and Swanepoel's method based on UV-Vis measurements. The refractive index was found to decrease over the thickness of the films. The number of the guiding modes increased with films' thickness as predicted by the dispersion curves and from that the cut-off thickness increased with the increase in films' thickness. This work emphasized the experimental consideration to be taken for the design of multimode slob waveguide based on $\mathrm{TiO_2}$ including the deposition method, thickness and refractive index. The high optical quality of our $\mathrm{TiO_2}$ thin films makes them very suitable for multimode waveguiding applications.

Competing Interests

There are no conflicts of interest between the authors.

References

[1] Bao-xing Zhao, Ji-cheng Zhou, and Lin-yan Rong. Microstructure and optical properties of TiO2 thin films deposited at different oxygen flow rates. *Transactions of Nonferrous Metals Society of China*, 20(8):1429–1433, August 2010.

[2] Sami Auvinen, Matti Alatalo, Heikki Haario, Erik Vartiainen, Juho-Pertti Jalava, and Ralf-Johan Lamminmäki. Refractive index functions of tio2 nanoparticles. *The Journal of Physical Chemistry C*, 117(7):3503–3512, 2013.

[3] Hai-Qing Jiang, Quan Wei, Quan-Xi Cao, and Xi Yao. Spectroscopic ellipsometry characterization of TiO2 thin films prepared by the sol–gel method. *Ceramics International*, 34(4):1039–1042, May 2008.

[4] Ghenadii Korotcenkov. *Titanium Dioxide (TiO2) and Its Applications*. Elsevier, 2020.

[5] Christopher C. Evans, Chengyu Liu, and Jin Suntivich. Low-loss titanium dioxide waveguides and resonators using a dielectric lift-off fabrication process. *Opt. Express*, 23(9):11160–11169, May 2015.

[6] I. Hegeman, M. Dijkstra, F. B. Segerink, W. Lee, and S. M. Garcia-Blanco. Development of low-loss TiO $_2$ waveguides. *Optics Express*, 28(5):5982, March 2020.

[7] J. Ben Naceur, M. Gaidi, F. Bousbih, R. Mechiakh, and R. Chtourou. Annealing effects on microstructural and optical properties of Nanostructured-TiO2 thin films prepared by sol–gel technique. *Current Applied Physics*, 12(2):422–428, March 2012.

[8] Karsten Pufahl, Dikran Boyaciyan, Jan Heckmann, Nicolai B. Grosse, Regine von Klitzing, and Ulrike Woggon. Symmetric cladding thin film waveguides: From lossy media to disordered nanostructures. *ACS Photonics*, 5(12):5110–5118, 2018.

[9] Adeel Afzal, Amir Habib, Iftikhar Ulhasan, Muhammad Shahid, and Abdul Rehman. Antireflective self-cleaning tio2 coatings for solar energy harvesting applications. *Frontiers in Materials*, 8:205, 2021.

[10] Juergen H. Braun, Andrejs Baidins, and Robert E. Marganski. Tio2 pigment technology: a review. *Progress in Organic Coatings*, 20(2):105–138, 1992.

[11] Md. Faruk Hossain, Subhagata Biswas, T. Takahashi, Y. Kubota, and A. Fujishima. Effect of substrate temperature on the photocatalytic activity of sputtered tio2thin film. *Physica Status Solidi (a)*, 205:2018–2022, 08 2008.

[12] Jenq-Nan Yih, Yi-Ming Chu, Yen-Chieh Mao, Wei-Han Wang, Fan-Ching Chien, Chun-Yu Lin, Kuang-Li Lee, Pei-Kuen Wei, and Shean-Jen Chen. Optical waveguide biosensors constructed with subwavelength gratings. *Appl. Opt.*, 45(9):1938–1942, Mar 2006.

[13] Francesco Arcadio, Luigi Zeni, Aldo Minardo, Caterina Eramo, Stefania Ronza, Chiara Perri, Girolamo D'Agostino, Guido Chiaretti, Giovanni Porto, and Nunzio Cennamo. A nanoplasmonic-based biosensing approach for wide-range and highly sensitive detection of chemicals. *Nanomaterials*, 11:1961, 07 2021.

[14] Harshini Mukundan, Aaron Anderson, W Grace, Karen Grace, Nile Hartman, Jennifer Martinez, and Basil Swanson. Waveguide-based biosensors for pathogen detection. *Sensors (Basel, Switzerland)*, 9:5783–809, 07 2009.

[15] Yuri Hayashi Isayama and Hugo Enrique Hernández-Figueroa. High-Order Multimode Waveguide Interferometer for Optical Biosensing Applications. *Sensors*, 21(9):3254, May 2021.

[16] M. F. Hossain, Puspita Paul, and T. Takahashi. Effect of deposition time on structural, optical and morphological properties of facing-target sputtered TiO2 thin film. In *2015 International Conference on Electrical & Electronic Engineering (ICEEE)*, pages 241–244, Rajshahi, Bangladesh, November 2015. IEEE.

[17] Ana Borras, Rafael Alvarez, Juan R. Sanchez-Valencia, Javier Ferrer, and Agustin R. Gonzalez-Elipe. Critical thickness and nanoporosity of tio2 optical thin films. *Microporous and Mesoporous Materials*, 160:1–9, 2012.

[18] Mohammed Shabat, Hala Khalil, Sofyan Taya, and M. Abadla. Analysis of the sensitivity of self-focused nonlinear optical evanescent waveguide sensors. *International Journal of Optomechatronics*, 1:284–296, 07 2007.

[19] Rahima Nasrin, Humayun Kabir, Hasina Akter, and A.H. Bhuiyan. Effect of film thickness on topographic, microstructural, optical and dielectric behaviour of ppmba thin films. *Results in Physics*, 19:103357, 2020.

[20] H Richter, ZP Wang, and L Ley. The one phonon raman spectrum in microcrystalline silicon. *Solid State Communications*, 39(5):625–629, 1981.

[21] I.H. Campbell and P.M. Fauchet. The effects of microcrystal size and shape on the one phonon Raman spectra of crystalline semiconductors. *Solid State Communications*, 58(10):739–741, June 1986.

[22] S. Balaji, Y. Djaoued, and J. Robichaud. Phonon confinement studies in nanocrystalline anatase-TiO2 thin films by micro Raman spectroscopy. *Journal of Raman Spectroscopy*, 37(12):1416–1422, December 2006.

[23] Agnès Pottier, Sophie Cassaignon, Corinne Chanéac, Françoise Villain, Elisabeth Tronc, and Jean-Pierre Jolivet. Size tailoring of TiO2 anatase nanoparticles in aqueous medium and synthesis of nanocomposites. Characterization by Raman spectroscopy. *Journal of Materials Chemistry*, 13(4):877–882, March 2003.

[24] Sergey Mamedov. Structural characterization of tio2 nanopowders by raman spectroscopy. *MRS Online Proceedings Library (OPL)*, 1806:1–6, 2015.

[25] Sergey Mamedov. Characterization of tio2 nanopowders by raman spectroscopy. *Spectroscopy*, 35:41, 06 2020.

[26] Y. Bouachiba, A. Taabouche, A. Bouabellou, F. Hanini, C. Sedrati, and H. Merabti. TiO $_2$ waveguides thin films prepared by sol-gel method on glass substrates with and without ZnO underlayer. *Materials Science-Poland*, 38(3):381–385, September 2020.

[27] F Medjaldi, A Bouabellou, Y Bouachiba, A Taabouche, K Bouatia, and H Serrar. Study of TiO2, SnO2 and nanocomposites TiO2:SnO2 thin films prepared by sol-gel method: Successful elaboration of variable–refractive index systems. *Materials Research Express*, 7(1):016439, jan 2020.

[28] B. Gharbi, Adel Taabouche, M. Brella, Rachid Gheriani, Y. Bouachiba, Abderrahmane Bouabellou, Faouzi Hanini, Samuel Louis Barouk, Houda Serrar, and Badis Rahal. Spray pyrolysis synthesized and zno–nio nanostructured thin films analysis with their nanocomposites for waveguiding applications. *Semiconductors*, 55:37–43, 2021.

[29] Julien Cardin and Dominique Leduc. Determination of refractive index, thickness, and the optical losses of thin films from prism-film coupling measurements. *Appl. Opt.*, 47(7):894–900, Mar 2008.

[30] R Swanepoel. Determination of the thickness and optical constants of amorphous silicon. *Journal of Physics E: Scientific Instruments*, 16(12):1214–1222, dec 1983.

[31] J C Manifacier, J Gasiot, and J P Fillard. A simple method for the determination of the optical constants n, k and the thickness of a weakly absorbing thin film. *Journal of Physics E: Scientific Instruments*, 9(11):1002–1004, nov 1976.

[32] Nuwat Pimpabute, Thanusit Burinprakhon, and Weerasak Somkhunthot. Determination of optical constants and thickness of amorphous GaP thin film. *Optica Applicata*, page 12, 01 2011.

[33] E.R. Shaaban, I.S. Yahia, and E.G. El-Metwally. Validity of Swanepoel's Method for Calculating the Optical Constants of Thick Films. *Acta Physica Polonica A*, 121(3):628–635, March 2012.

[34] T. Sekiya, S. Ohta, S. Kamei, M. Hanakawa, and S. Kurita. Raman spectroscopy and phase transition of anatase tio2 under high pressure. *Journal of Physics and Chemistry of Solids*, 62(4):717–721, 2001.

[35] Masayoshi Mikami, Shinichiro Nakamura, Osamu Kitao, and Hironori Arakawa. Lattice dynamics and dielectric properties of $\mathrm{tio_2}$ anatase: A first-principles study. *Phys. Rev. B*, 66:155213, Oct 2002.

[36] E.J. Ekoi, A. Gowen, R. Dorrepaal, and D.P. Dowling. Characterisation of titanium oxide layers using raman spectroscopy and optical profilometry: Influence of oxide properties. *Results in Physics*, 12:1574–1585, 2019.

[37] A. Naumenko, Iu. Gnatiuk, N. Smirnova, and A. Eremenko. Characterization of sol–gel derived TiO2/ZrO2 films and powders by Raman spectroscopy. *Thin Solid Films*, 520(14):4541–4546, May 2012.

[38] M. Šćepanović, M. Grujić-Brojčin, Z. Dohčević-Mitrović, and Zoran V. Popović. Effects of Confinement, Strain and Nonstoichiometry on Raman Spectra of Anatase TiO_2 Nanopowders. *Materials Science Forum*, 518:101–106, July 2006.

[39] John C. Parker and Richard W. Siegel. Calibration of the raman spectrum to the oxygen stoichiometry of nanophase tio2. *Applied Physics Letters*, 57:94–945, 1990.

[40] Svetlana V. Rempel, Andrey A. Rempel, and Albina A. Valeeva. Effect of Stoichiometry and Ordering on the Microstructure of Titanium Monoxide $\mathrm{TiO_y}$. *ACS Omega*, 5(35):22513–22519, September 2020.

[41] M.M. Abdel-Aziz, I.S. Yahia, L.A. Wahab, M. Fadel, and M.A. Afifi. Determination and analysis of dispersive optical constant of TiO2 and Ti2O3 thin films. *Applied Surface Science*, 252(23):8163–8170, September 2006.

[42] Kristel Möls, Lauri Aarik, Hugo Mändar, Aarne Kasikov, Ahti Niilisk, Raul Rammula, and Jaan Aarik. Influence of phase composition on optical properties of TiO2: Dependence of refractive index and band gap on formation of TiO2-II phase in thin films. *Optical Materials*, 96:109335, October 2019.

[43] Hougang Fan, Dandan Chen, Xuefeng Ai, Shuo Han, Maobin Wei, Lili Yang, Huilian Liu, and Jinghai Yang. Mesoporous tio2 coated znfe2o4 nanocomposite loading on activated fly ash cenosphere for visible light photocatalysis. *RSC Adv.*, 8:1398–1406, 2018.

[44] Yahia Djaoued, K. Ozga, A. Wojciechowski, A.H. Reshak, J. Robichaud, and I.V. Kityk. Photoinduced effects in tio2 nanocrystalline films with different morphology. *Journal of Alloys and Compounds*, 508(2):599–605, 2010.

[45] Yosuke Kayanuma. Quantum-size effects of interacting electrons and holes in semiconductor microcrystals with spherical shape. *Phys. Rev. B*, 38:9797–9805, Nov 1988.

[46] I. A. Shvets, I. I. Klimovskikh, Z. S. Aliev, M. B. Babanly, J. Sánchez-Barriga, M. Krivenkov, A. M. Shikin, and E. V. Chulkov. Impact of stoichiometry and disorder on the electronic structure of the PbBi 2 Te 4 - x Se x topological insulator. *Physical Review B*, 96(23):235124, December 2017.

[47] Jie Deng and Zong-Yan Zhao. Effects of non-stoichiometry on electronic structure of Cu $_{x}$ S $_{y}$ compounds studied by first-principle calculations. *Materials Research Express*, 6(10):105513, August 2019.

[48] Haowei Peng, Jingbo Li, Shu-Shen Li, and Jian-Bai Xia. First-principles study of the electronic structures and magnetic properties of 3d transition metal-doped anatase TiO $_{2}$. *Journal of Physics: Condensed Matter*, 20(12):125207, March 2008.

[49] Xiaolan Kang, Sihang Liu, Zideng Dai, Yunping He, Xuezhi Song, and Zhenquan Tan. Titanium dioxide: from engineering to applications. *Catalysts*, 9(2):191, 2019.

[50] Tahar Touam, Lamia Znaidi, Dominique Vrel, Iva Ninova-Kuznetsova, Ovidiu Brinza, Alexis Fischer, and Azzedine Boudrioua. Low loss sol-gel tio2 thin films for waveguiding applications. *Coatings*, 3(1):49–58, 2013.

[51] Andreas Jamnig, D. Sangiovanni, Grégory Abadias, and Kostas Sarakinos. Atomic-scale diffusion rates during growth of thin metal films on weakly-interacting substrates. *Scientific Reports*, 9:6640, 04 2019.

[52] Navina Mehan, Monika Tomar, Vinay Gupta, and Abhai Mansingh. Optical waveguiding and birefringence properties of sputtered zinc oxide (zno) thin films on glass. *Optical Materials*, 27(2):241–248, 2004.

[53] David K. Teertstra. Photon refraction in dielectric crystals using a modified gladstone-dale relation. *The Journal of Physical Chemistry C*, 112(20):7757–7760, 2008.

[54] D. Burnett. The relation between refractive index and density. *Mathematical Proceedings of the Cambridge Philosophical Society*, 23(8):907–911, 1927.

[55] Xavier Rocquefelte, Fabrice Goubin, Hyun-Joo Koo, Myung-Hwan Whangbo, and Stéphane Jobic. Investigation of the origin of the empirical relationship between refractive index and density on the basis of first principles calculations for the refractive indices of various tio2 phases. *Inorganic Chemistry*, 43(7):2246–2251, 2004. PMID: 15046498.

[56] S Swann. Film thickness distribution in magnetron sputtering. *Vacuum*, 38(8):791–794, 1988.

[57] Micael Oliveira, Alberto Castro, Miguel Marques, and Angel Rubio. On the use of neumann's principle for the calculation of the polarizability tensor of nanostructures. *Journal of nanoscience and nanotechnology*, 8:3392–8, 08 2008.

[58] H.-J. Weber. Anisotropic bond polarizabilities in birefringent crystals. *Acta Crystallographica Section A*, 44(3):320–326, May 1988.

[59] Sven Lidin. Mapping bond orientations with polarized x-rays. *Science*, 344(6187):969–970, 2014.

[60] A.T. Amos and R.J. Crispin. Bond contributions to molecular refractive indices and verdet constants. *Molecular Physics*, 31(1):147–158, 1976.

[61] David R. Lide. *CRC Handbook of Chemistry and Physics, 90th Edition*. Taylor & Francis, 2009.

[62] Mark Fox. *Optical properties of solids*. Number v. 3 in Oxford master series in condensed matter physics. Oxford University Press, Oxford ; New York, 2nd ed edition, 2010.